Computational Materials Science 49 (2010) 568–581

Contents lists available at ScienceDirect

Computational Materials Science

journal homepage: www.elsevier.com/locate/commatsci

Computing mechanical response variability of polycrystalline microstructures through dimensionality reduction techniques

Zheng Li [b,a], Bin Wen [a], Nicholas Zabaras [a,*]

[a] Materials Process Design and Control Laboratory, Sibley School of Mechanical and Aerospace Engineering, 101 Frank H. T. Rhodes Hall, Cornell University, Ithaca, NY 14853-3801, USA
[b] State Key Laboratory of Structural Analysis for Industrial Equipment, Faculty of Vehicle Engineering and Mechanics, Dalian University of Technology, Dalian 116024, China

ARTICLE INFO

Article history:
Received 22 March 2010
Received in revised form 15 May 2010
Accepted 27 May 2010
Available online 30 June 2010

Keywords:
Polycrystalline microstructures
Nonlinear model reduction
Homogenization
Microstructure reconstruction
Stochastic analysis
Karhunen–Loève Expansion
Texture

ABSTRACT

Many areas of material science involve analyzing and linking the material microstructure with macroscale properties. Constructing low-dimensional representations of microstructure variations would greatly simplify and accelerate materials design and analysis tasks. We develop a mathematical strategy for the data-driven generation of low-dimensional models that represents the variability in polycrystal microstructures while maintaining the statistical properties that these microstructures satisfy. This strategy is based on a nonlinear dimensionality reduction framework that maps the space of viable grain size variability of microstructures to a low-dimensional region and a linear dimensionality reduction technique (Karhunen–Loève Expansion) to reduce the texture representation. This methodology allows us to sample microstructure features in the reduced-order space thus making it a highly efficient, low-dimensional surrogate for representing microstructures (grain size and texture). We demonstrate the model reduction approach with polycrystal microstructures and compute the variability of homogenized properties using a sparse grid collocation approach in the reduced-order space that describes the grain size and orientation variability.

1. Introduction

Mathematical representation of microstructures is essential for allowing microstructure-sensitive design applications (optimizing microstructures leading to optimal properties) [1], exploring microstructure/property/process spaces [2], computing error-bars of materials properties induced by microstructural uncertainty [3,4], allowing multiscale modeling, among others. Concurrently, recent advances in high throughput characterization of polycrystalline microstructures have resulted in huge data sets of microstructural descriptors and image snapshots. To efficiently utilize these large scale experimental data for the above mentioned applications, it is important to efficiently compress the data into low-dimensional models.

In this work, a microstructure is described by its grain size and texture. Our interest is on *constructing reduced-order representations of polycrystalline microstructures based on available experimental or simulation-based data* (microstructural snapshots). Given a set of microstructures having the same constituent elements and the same processing history, each microstructure may be visually different from another, but will satisfy some statistical correlations that inherently define its material distribution (volume fraction of one constituent element) and/or the processing history (a specific grain size distribution and preferred texture). Instead of storing and manipulating this large data set of microstructures directly, a reduced-order model that satisfies and respects these statistical correlations while efficiently encoding and quantifying the variations in this data set would significantly accelerate and simplify analysis. This low-dimensional model can then be used to completely represent the microstructure variability.

In earlier work [5], we developed a linear embedding methodology to model the topological variations of composite microstructures satisfying some experimentally determined statistical correlations. A model reduction scheme based on Principal Component Analysis (PCA) was developed. This model was successful in reducing the representation of two-phase microstructures. However, as most of the data sets contain essential nonlinear structures that are invisible to PCA, it cannot be easily extended to the case of polycrystals.

In [6], a nonlinear dimensionality reduction (NLDR) strategy was proposed to embed data variations into a low-dimensional manifold that could serve as the input model for subsequent analysis. This methodology was applied to construct a reduced-order model of thermal property variation of a two-phase microstructure. The model was subsequently utilized as a stochastic input model to study the effect of material uncertainty on thermal

* Corresponding author. Fax: +1 607 255 1222.
E-mail address: zabaras@cornell.edu (N. Zabaras).
URL: http://mpdc.mae.cornell.edu/ (N. Zabaras).

0927-0256/$ - see front matter © 2010 Elsevier B.V. All rights reserved.
doi:10.1016/j.commatsci.2010.05.051

diffusion. Our focus in this paper is to extend this nonlinear dimensionality reduction methodology to develop a low-dimensional representation of *polycrystalline microstructures with attention given at present to grain size distribution*. This problem poses significant challenges, particularly the following: (a) The low-dimensional model must have the ability to reconstruct the grain sizes of different microstructures, (b) this can be incorporated by using a notion of distance between microstructures [6], however the choice of the distance metric is not straight forward, and (c) the low-dimensional model must be able to interpolate between two microstructures (construct a microstructure between two neighboring (in the sense of the metric used) microstructures). This last item is important as our goal is to be able to sample in the reduced-order surrogate microstructure space for estimating property variations induced by microstructure uncertainty.

Besides grain size, material properties of polycrystalline microstructures are also highly dependent on their texture. The texture of a microstructure is usually represented by a set of axis-angle described orientations (Rodrigues parametrization) of individual grains. Each orientation contains three components, which can be totally random if no information is assumed. In reality, however, materials usually acquire certain preferred texture after processing. This introduces correlations among grain orientations and enable us to perform model reduction techniques on the texture. Some linear approaches have shown success in reducing Orientation Distribution Function (ODF) [7–9], where the mechanical properties of the microstructure were updated based on the evolution of ODF according to a conservation equation, in which the microstructure was assumed to be continuous. In this paper, a discrete microstructure model is adopted, in which the texture is consisted of finite number of orientations. Karhunen–Loève Expansion (KLE) is directly applied to pre-processed grain orientations. The change of the texture and therefore the material properties correspond to elastic distortion inside the microstructure domain. The grain size feature is assumed here to be independent of texture. Therefore, model reduction is applied to them separately. After reducing both grain size and texture, the low-dimensional representation is transformed to a hypercube where sampling techniques such as sparse grid collocation [10] can be applied with high efficiency.

One of our interests is in computing the variability (e.g. the probability distribution function (PDF)) of macroscopic mechanical response of a polycrystal (e.g. stress/strain response) subjected to homogenized compression. The grain size distribution is given in terms of moments (e.g. 1st-moment refers to mean volume, second-moment determines standard deviation and higher-order moments further constrain the grain size distribution), and the initial texture is assumed to be obtained from certain random process. Here, we consider that the property of interest F is a function of grain size distribution and texture, $F(\mathrm{GS},\mathrm{TX})$. We are interested to compute the PDF, $P(F)$. Our basic approach is first to solve a series of stochastic partial differential equations (SPDEs) controlling the material property evolution using the sparse grid collocation method that constructs an interpolant of the microstructure mechanical response in the stochastic space. Then, the material response is fully defined in the stochastic space using the interpolation basis functions. One can easily construct a histogram and the PDF can be computed through Kernel Density Estimation [11].

In [3], the Maximum Entropy method was used to quantify the stress response uncertainty due to microstructure variation. Even though both approaches are data-driven, the methodology discussed in this paper produces an interpolant (with quantifiable error) of the stress/strain response in the stochastic space of grain size distribution and texture. This interpolant allows us to compute the stochastic stress/strain response of any other (interpolated) microstructure in the space of allowable microstructures. The MaxEnt on the other hand provides a distribution from which viable microstructures can be sampled and interrogated to produce via Monte Carlo methods the statistical moments of the stress/strain response. In addition, the work in [3] did not explicitly account for grain size effects in the crystal plasticity model employed.

The outline of this paper is as follows: In the next section, the central idea of the nonlinear dimension reduction strategy is described. Section 3 introduces a grain size measurement of microstructures and a methodology of interpolating polycrystalline microstructures leading to viable microstructures that satisfy the statistical grain size distribution correlations. Section 4 introduces the Karhunen–Loève Expansion on texture space. Section 5 briefly reviews the Adaptive Sparse Grid Collocation method for solving problems governed by stochastic differential equations. The crystal plasticity deterministic solver is briefly described in Section 6. Section 7 presents several examples demonstrating the various steps of the approach and the propagation of the microstructural uncertainty in the variability of homogenized mechanical properties. We conclude in Section 8 with a brief discussion on open issues and future avenues of research.

2. Model reduction theory

Features of polycrystals are composed of two aspects: topology and texture. The first aspect regards geometry characters, such as grain shape and grain size, while the second is the orientation distribution of grains. For a polycrystalline microstructure, its material properties are mostly determined by the grain size and orientation distribution. In order to model the uncertainty of microstructures, the two features are considered as random fields. Model reduction techniques are applied to grain size and texture separately, and then their low-dimensional representations are combined to fully represent a microstructure. In this section, focus is given on a nonlinear model reduction scheme performing on the grain size space. The model reduction on texture will be introduced in Section 4.

Fig. 1 shows multiple microstructures that satisfy some specific experimentally determined statistics of grain size distribution. Each microstructure that satisfies the given statistics of the grain size distribution is a point that lies on a curve (manifold) embedded in a high-dimensional space. The problem of 'manifold learning' as applied to this situation is as follows: *given a set of N unordered points belonging to a manifold $\mathscr{M}$ embedded in a high-dimensional space $\mathbb{R}^n$, find a low-dimensional region $\mathscr{A} \subset \mathbb{R}^{d_1}$ that parameterizes $\mathscr{M}$, where $d_1 \ll n$.*

The process of learning the nonlinear low-dimensional structure hidden in a set of unorganized high-dimensional data points is known as the *manifold learning problem*. Principal Component Analysis (PCA), Karhunun–Loève Expansion (KLE) and Multi-Dimensional Scaling (MDS) [12] are classical methods in manifold learning. These methods extract optimal mappings when the manifold is embedded linearly or almost linearly in the input space. However, in most cases of interest, the manifold is nonlinearly embedded in the input space, making the classical methods of dimension reduction highly approximate.

Recently two new approaches have been developed that combine the computational advantages of PCA with the ability to extract the geometric structure of nonlinear manifolds. One set of methods takes a bottom-up approach, i.e they try to preserve the local geometry of the data. They aim to map nearby points on the manifold to nearby points in the low-dimensional representation. Such methods, Locally Linear Embedding (LLE) [13], Laplacian Eigen Maps, Hessian Eigen Maps, essentially construct a homeomorphic mapping between local sets in the manifold to an open ball in a low-dimensional space. The complete mapping is a union

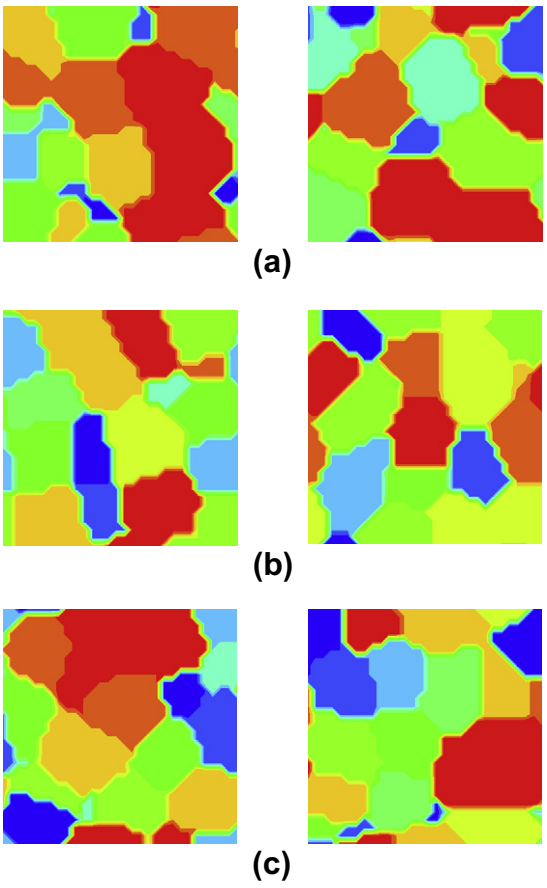

Fig. 1. Slices of 3D microstructures satisfying different constraints of the grain size (given here in terms of grain volume, the domain of microstructure is 1 mm^3) distribution: (a) constant mean grain volume (0.0185 mm^3), (b) constant mean grain size (0.0185 mm^3) and second-order moment (3.704×10^{-4} mm^6), and (c) constant grain size (0.0185 mm^3), second-order moment (3.704×10^{-4} mm^6) and third-order moment (8.637×10^{-6} mm^9).

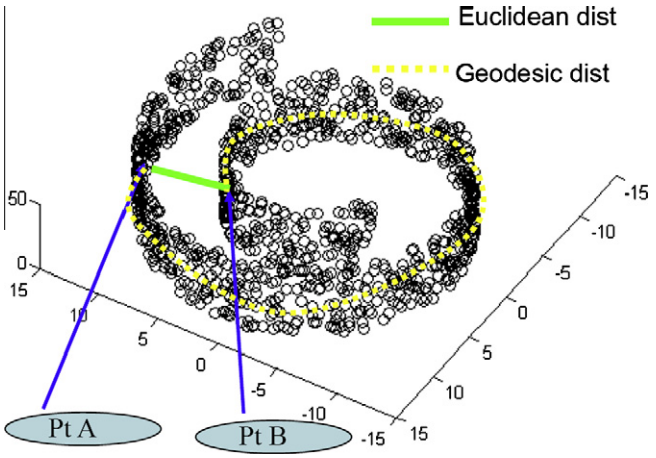

Fig. 2. A schematic showing the manifold in the high- and low-dimensional spaces. The data points shown here are in 3D but the intrinsic dimensionality of the manifold is two.

of these local maps. On the other hand, the alternate set of approaches towards nonlinear model reduction take a top-down approach [14]. Such global approaches, like the Isomap and its numerous variants, attempt to preserve the geometry at all scales. They ensure that nearby points on the manifold (with distance defined via a suitable metric) map to nearby points in the low-dimensional space and faraway points map to faraway points in the low-dimensional space. The distance between original points is identical to that between their low-dimensional counterparts. Though both approaches are viable, we focus our attention in the current work to global methods of nonlinear dimension reduction.

The basic premise of the Isomap [15,16] algorithm is that 'only geodesic distances reflect the true low-dimensional geometry of the manifold'. The geodesic distance (between two points) on a manifold can be intuitively understood to be the shortest distance between the two points *along the manifold* (see Fig. 2 for an illustration).

Subsequent to the construction of the geodesic distance between the sample points $\{\mathbf{x}_i\}$ in the high-dimensional space, the Isomap [15] algorithm constructs the low-dimensional parametrization simply as a set of points $\{\mathbf{y}_i\}$ lying in a low-dimensional space that most accurately preserve the geodesic distance. That is, the distance between two points $\mathbf{y}_i$ and $\mathbf{y}_j$ in low-dimensional space should be the same with the geodesic distance between their corresponding points $\mathbf{x}_i$ and $\mathbf{x}_j$ in the high-dimensional space. This property is called isometry. With the Isomap algorithm, *given a set of N-unordered points belonging to a manifold $\mathscr{M}$ embedded in a high-dimensional space $\mathbb{R}^n$, a low-dimensional region $\mathscr{A} \in \mathbb{R}^{d_1}$ is computed which is isometric to $\mathscr{M}$, with $d_1 \ll n$.*

Since we have no notion of the geometry of the manifold to start with (hence cannot construct the true geodesic distances), we approximate the geodesic distance using the concept of graph distance $\mathscr{D}_G(i,j)$, thus the distance of points far away is computed as a sequence of small hops. This approximation, $\mathscr{D}_G(i,j)$, asymptotically matches the actual geodesic distance $\mathscr{D}_M(i,j)$ in the limit of large number of samples [6]. As discussed before, the key to a good model reduction and reconstructions is a viable measurement of microstructure. Since the important feature we are looking to embed and recreate is the grain size distribution, we choose this feature as the measurement (see Section 3).

Having computed the pairwise distance matrix between the given microstructures, one can compute the location of N points in a reduced-order surrogate space, $\mathbf{y}_i \in \mathbb{R}^{d_1}$ such that the distance between these points is arbitrarily close to the given distance matrix. Multi-Dimensional Scaling (MDS) methods allow this mapping [6]. The intrinsic dimension d_1 of an embedded manifold is linked to the rate of convergence of the length functional of the minimal spanning tree of the geodesic distance matrix of the unordered data points in the high-dimensional space [6]. The rate of change of the length functional as more number of points are chosen is related to the dimensionality of the manifold via a simple relation $log(L) = alog(N) + \epsilon$, where $a = (d_1 - 1)/d_1$. The intrinsic dimensionality, d_1, can be estimated by finding the length functional for different number of samples N and subsequently finding the best fit for a.

The procedure above results in N points in a low-dimensional space $\mathbb{R}^{d_1}$. The geodesic distance and the MDS step result in a low-dimensional convex region $\mathscr{A} \subset \mathbb{R}^{d_1}$. Using the N samples, the reduced space is given as a convex hull $\mathscr{A} = \text{convex hull}(\mathbf{y}_i)$ that parameterizes the grain size space. Since microstructures in $\mathscr{M}$ satisfy all the required grain size properties, they are here taken to be equally probable to occur. That is, every point in the high-dimensional stochastic space $\mathscr{M}$ is equiprobable. The convex hull can be mapped to a unit hypercube with the same dimensionality d_1. Since the microstructures are equiprobable, we consider each of the dimensions of the hypercube as defining an independent uniform random variable. These random variables define our stochastic support space. Since $\mathscr{A}$ serves as the surrogate space of $\mathscr{M}$, we can access the variability in $\mathscr{M}$ by sampling over $\mathscr{A}$, or equivalently the hypercube, which is the sampling space in the

sparse grid collocation method. Unfortunately, this requires not only the mapping $\mathscr{M} \rightarrow \mathscr{A}$ just described but also the inverse mapping (microstructure reconstruction) $\mathscr{A} \rightarrow \mathscr{M}$. This microstructure reconstruction will be discussed in Section 3.2. The overall steps of the procedure are summarized in Fig. 3. Note that here the surrogate space $\mathscr{A}$ is mapped to a unit d_1 – dimensional hypercube to allow interfacing this procedure with sparse grid collocation techniques [10]. In such collocation methods, the sampling points are defined on a hypercube. These collocation methods have been shown to be efficient in interfacing with deterministic solvers of e.g. deformation, diffusion, flow, etc. in random media, thus allowing modeling the effect of microstructural uncertainty on material properties.

3. Microstructure representation and reconstruction methodology

3.1. Microstructure representation: grain size vector of a microstructure

The high-dimensional representation of a microstructure topology feature in this paper is chosen to be the grain size distribution, namely the volume of grains, for its great effect on mechanical properties of a microstructure. A polycrystalline microstructure contains a finite number of grains and each grain has its own size. If the size of each grain is given, the microstructure can be non-uniquely determined. The only differences in geometry of these microstructures are the shapes and arrangement of the grains, which do not have significant effect on microstructure mechanical properties and can be neglected especially when the Taylor homogenization hypothesis is adopted. Here, we treat microstructures having the same grain size distribution to be in the same class. A measurement that uniquely represents this kind of microstructures is needed. In this paper, the measurement is chosen as the grain size (in terms of volume) vector sorted by ascending order (we refer it as 'sorted grain size vector') and the term 'microstructure' in the following refers to the grain size feature instead of a microstructure realization. For example, consider a cubic microstructure containing $n = 4$ grains whose volumes are given as $GS = \{0.3\ mm^3, 0.2\ mm^3, 0.4\ mm^3, 0.1\ mm^3\}$. Rearranging the grain size in ascending order, the new representation of this microstructure is $GS = \{0.1\ mm^3, 0.2\ mm^3, 0.2\ mm^3, 0.4\ mm^3\}$. This resulting vector is chosen as the representation of this kind of microstructure. After being sorted, microstructures belonging to the same class result in the same grain size vector, while different classes give different vectors. This choice is selected as it is easy to express and satisfy the given constraints on grain size (mean, standard deviation, higher-order moments, etc.) and in addition, the (non-unique) reconstruction of a microstructure with given grain sizes is straightforward. In the meantime, adopting Euclidean distance as the metric, we can measure the difference between microstructures represented by sorted grain size vector. To estimate the difference between two microstructures, $\mathbf{A} \in \mathscr{M}$ and $\mathbf{B} \in \mathscr{M}$, we first sort the grain sizes (effectively, grain volume) by ascending order. The Euclidean distance, $\mathscr{D}_G(\mathbf{A}, \mathbf{B})$, between them is defined as follows:

$$\mathscr{D}(\mathbf{A}, \mathbf{B}) = \left(\sum_i^n \left(GS_i^A - GS_i^B \right)^2 \right)^{1/2} \tag{1}$$

Fig. 4 shows an example of using sorted grain size vector to measure the difference between two 54-grain microstructures. Fig. 4a depicts the sorted grain volume distribution of two microstructures having the same mean grain size. Fig. 4b measures the difference in each grain between the microstructures, which also tells how much microstructure **A** is different from microstructure **B**. The dimensionality of this grain size vector is determined by the number of grains of a microstructure. For a microstructure containing 54 grains, its representation is 54-dimensional. As the mean grain size is fixed, there are only 53 independent dimensions. If more constraints are added, the dimensionality will be further reduced.

3.2. Microstructure reconstruction

Given a set of samples $\{\mathbf{x}_i\}$, $i = 1, \ldots, N$ in manifold $\mathscr{M}$, the nonlinear dimensionality reduction strategy (Section 2) convert these points into a set of points $\{\mathbf{y}_i\}$, $i = 1, \ldots, N$ belonging to a convex set $\mathscr{A}$. This convex region $\mathscr{A} \subset \mathbb{R}^{d_1}$, defines the reduced representation of the space of microstructures. As $\mathscr{A}$ is the surrogate space of $\mathscr{M}$, one can access the complete variability in the topology and property distribution of grain size in $\mathscr{M}$ by simply sampling over

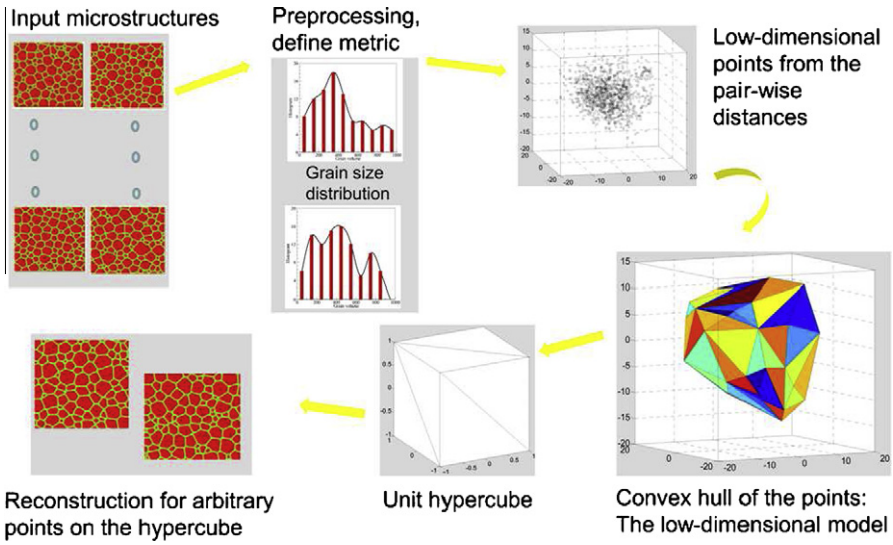

Fig. 3. The various steps in a data-driven model reduction of polycrystal microstructures. The high-dimensional microstructures are mapped to a low-dimensional region $\mathscr{A}$. This convex region defined by the data points in $\mathscr{A}$ is mapped to a unit hypercube. Each sample point on this hypercube corresponds to a viable microstructure that needs to be reconstructed using the given data.

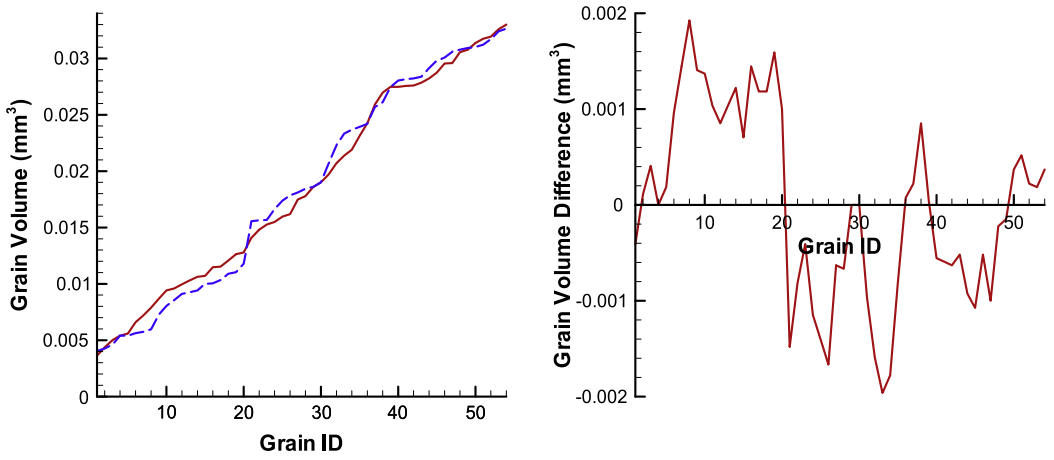

Fig. 4. (a) Two microstructures represented by sorted grain size vectors. (b) The difference between the two sorted grain size vectors.

the region $\mathscr{A}$. But we have no knowledge of the image of a point in the microstructural space $\mathscr{M}$ corresponding to an arbitrary point $\mathbf{y} \in \mathscr{A}$. For a usable reduced-order model of the microstructure space, an explicit mapping $\mathscr{F}^{-1}$ from $\mathscr{A}$ to $\mathscr{M}$ has to be constructed.

As shown in Fig. 3, the reduced-dimensionality space $\mathscr{A}$ is used as the surrogate space from which acceptable microstructures need to be sampled (at arbitrary points). The procedure of reconstructing a microstructure $\mathbf{x} \in \mathscr{M}$ from the low-dimensional space $\mathscr{A} \subset \mathbb{R}^{d_1}$ is as follows: (1) Generate a point in the low-dimensional space $\mathbf{y} \in \mathscr{A}$. (2) Find the m nearest neighbors of $\mathbf{y}$ and denote them as $\mathbf{y}_i, i = 1,\ldots,m$. (3) Find the microstructures $\mathbf{x}_i, i = 1,\ldots,m$ in the high-dimensional space $\mathscr{M} \subset \mathbb{R}^n$ that are corresponding to $\mathbf{y}_i$, $i = 1,\ldots,m$. Based on isometry, $\mathbf{x}$ could be computed following a linear interpolation algorithm:

$$\mathbf{x} = \sum_{i=1}^{m} W_i \mathbf{x}_i, \quad W_i = \frac{\frac{1}{\mathscr{D}(\mathbf{y}_i,\mathbf{y})}}{\sum_{j=1}^{m} \frac{1}{\mathscr{D}(\mathbf{y}_j,\mathbf{y})}} \tag{2}$$

Note that the metric in the reduced space $\mathscr{A} \subset \mathbb{R}^{d_1}$ is the Euclidean distance and the points $\mathbf{x}_i \in \mathscr{M}$ were the sorted grain size vectors defined earlier. The equation above demonstrates that the new generated microstructure can be interpolated by its nearest neighbors weighed by the reciprocal distances between their corresponding low-dimensional points. The mean grain size of the interpolated microstructure automatically equals the required value because of the linearity of Eq. (2). However, when the microstructures on the manifold are constrained by higher-order moments, the resulted microstructure by interpolation cannot satisfy all the constraints, which means it does not lie on the manifold, but has slight deviation. To obtain the microstructure satisfying all the given moments, we need to modify the grain sizes. This procedure is referred to as projecting the image onto the manifold in [6]. An algorithm implemented in the current work that can adjust the grain size distribution to satisfy the second- and third-moments of grain size is briefly described below.

Controlling the grain size distribution to satisfy a given second-order moment of the grain size distribution is straightforward. Given a grain size vector whose mean size is M_1, we would like to adjust the grain sizes so that its second-order moment is M_2. To do this, we first transform the original grain size vector to one that has zero mean by subtracting M_1 from each component. We next weight each component with the ratio of the expected standard deviation to the current standard deviation. The algorithm is as follows:

Step 1: $E_1 = \frac{1}{n}\sum_{i=1}^{n} S_i = M_1$;

Step 2: $S_i = S_i - M_1$;

Step 3: $E_2 = \frac{\sum_{i=1}^{n} S_i^2}{n}$;

Step 4: $a = \sqrt{\frac{M_2 - M_1^2}{E_2}}$;

Step 5: $S_i = aS_i$.

Having the zero-mean grain size vector satisfying the expected standard deviation, the final grain size vector that satisfies both the mean size and second-order moment can be obtained by adding M_1 to its components, i.e. $S_i = M_1 + aS_i$, for $i = 1,\ldots,n$.

The control the third-order moment is more complicated. Two iterative processes are needed to accomplish this task. The basic idea is to find an intersection vector of two surfaces. One surface is composed of microstructures satisfying the first two moments and the other one is defined by the third-order moment M_3. Still, the mean size M_1 is subtracted from the grain size vector. The first three target moments of the zero-mean grain size vectors are then equal to $\widehat{M}_1 = 0$, $\widehat{M}_2 = M_2 - M_1^2$, and $\widehat{M}_3 = M_3 - 3M_1M_2 + 2M_1^3$, respectively. The complete algorithm is as follows:

Step 1: $\widehat{S}_i = S_i - M_1$;
Step 2: $\widehat{S}_i' = \widehat{S}_i$, and $E_1 = \frac{1}{n}\sum_{i=1}^{n} S_i$;
Step 3: $\widehat{S}_i = \widehat{S}_i - E_1$;
Step 4: $E_2 = \frac{1}{n}\sum_{i=1}^{n} S_i^2$;
Step 5: $\widehat{S}_i = \widehat{S}_i \sqrt{\frac{\widehat{M}_2}{E_2}}$;
Step 6: loop

$$\delta_i = \frac{3\widehat{S}_i^2}{n};$$
$$d = \sum_{i=1} n\delta_i^2, \quad E_3 = \frac{1}{n}\widehat{S}_i^3;$$
$$m = \widehat{M}_3 - E_3;$$
$$\widehat{S}_i = \widehat{S}_i + \frac{m}{d}\delta_i;$$
if $|m| <$ cutoff, break;

Step 7: error $= \mathrm{norm}(\widehat{S}_i' - \widehat{S}_i)$;
Step 8: if error < cutoff, go to step 9, else go to step 1;
Step 9: $S_i = M_1 + \widehat{S}_i$.

The grain size vector $\{S_i, i = 1,\ldots,n\}$ now satisfies all the three given moment constraints.

Reconstruction of a microstructure with a known grain size distribution is a difficult inverse problem and for this task, one can employ a combination of grain growth simulation methods including phase-field methods [17]. In the current work, the

realization of the 3D microstructure is not necessary. An example of a 3D microstructure that satisfies given moment constraints is shown in Fig. 5.

Given the methodology discussed in Sections 2 and 3, the mapping between high- and low-dimensional stochastic space of grain size feature is constructed based on a isometric nonlinear model reduction methodology. In the next section, the representation and model reduction on texture space will be introduced.

4. Texture modeling

Other than grain size, the properties of a polycrystalline microstructure are highly dependent on its texture. For the case of a discrete microstructure containing moderate number of grains, the texture effect is usually much more significant than the grain size effect. To examine the effect of variability in initial texture on the final property of the microstructure, the texture is defined as a random field, whose variables are orientation components of the individual grains. In this paper, the orientation of a grain is defined by a rotation around an axis and is known as Rodrigues parametrization, an axis-angle representation consisted of three components:

$$\mathbf{r} = \mathbf{w} tan\frac{\phi}{2} \tag{3}$$

where $\mathbf{r} = \{r_1, r_2, r_3\}$ are the three Rodrigues components; $\mathbf{w} = \{w_1, w_2, w_3\}$ gives the direction cosines of the rotation axis with respect to microstructure coordinates; and ϕ is the rotation angle.

In nature, the orientation of a grain should be totally random if no constraint is taken into account. Through certain deformation, the orientation is changed due to grain rotation and distortion, and therefore forms preferred texture throughout the entire microstructure. For a set of independently randomly distributed orientations, it is difficult to perform dimensionality reduction because of lack of intrinsic correlations. However, processed microstructures through certain deformation mode gain preferred texture that are implicitly correlated among orientations. Several linear dimensionality reduction techniques have already been successfully implemented in reducing the Orientation Distribution Function (ODF) to lower-dimensional representations [7,9]. In those works, the material deformation simulation was conducted using an ODF based scheme, where the microstructure was assumed to be continuous and its macroscopic properties were computed by integrating over the entire fundamental zone of Rodrigues space. The ODF was updated following the ODF conservation equation [18].

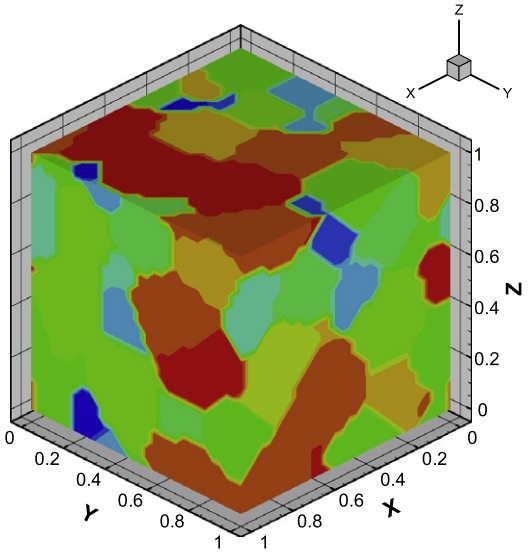

Fig. 5. A 3D microstructure with 64 grains with prescribed mean grain size value (0.015625 mm^3). The reconstruction is based on a grain-growth model implemented using a phase-field method.

In the current work, however, the microstructure is discretely represented by an ensemble of grains, each of which possesses an orientation consisted of three axis-angle parameters (Eq. (3)). The update of the texture is obtained by estimating the elastic distortion inside the grains [19]

$$\begin{aligned}\mathbf{m}_t^\alpha &= \mathbf{F}^e(t)\mathbf{m}_0^\alpha \\ \mathbf{n}_t^\alpha &= \mathbf{F}^{e-T}(t)\mathbf{n}_0^\alpha\end{aligned} \tag{4}$$

where $\mathbf{m}^\alpha$, $\mathbf{n}^\alpha$ are the direction and normal of the slip system α and $\mathbf{F}^e$ is the elastic deformation gradient. In this case, the texture is described by a finite number of orientations (the same with grain number), leading only certain points in Rodrigues space having a non-zero ODF value. Thus, the appropriate method to reduce the texture dimension should be directly preformed on grain orientations, instead of assuming a continuous field in Rodrigues space.

Here, we define the orientation vector representing the microstructure texture as

$$\boldsymbol{\tau}(\mathbf{r}) = \left\{r_1^1, r_2^1, r_3^1, r_1^2, r_2^2, r_3^2, \ldots, r_1^n, r_2^n, r_3^n\right\}^T \tag{5}$$

where n is the total number of grains. Texture $\boldsymbol{\tau} \in \mathscr{T}$, in which $\mathscr{T} \subset \mathbb{R}^{3n}$ is the stochastic space of texture. The Rodrigues representation is defined in Eq. (3). $\{r_1^i, r_2^i, r_3^i\}$ are the three orientation components of the ith grain. The initial orientations of grains are provided in the form of Eq. (5) through input files. The initial orientation matrix of grain i ($i = 1, \ldots, n$) can be calculated by

$$\mathbf{R}_0^i = \frac{1}{1 + \mathbf{r}_0^i \cdot \mathbf{r}_0^i}\left(\mathbf{I}\left(1 - \mathbf{r}_0^i \cdot \mathbf{r}_0^i\right) + 2\left(\mathbf{r}_0^i \otimes \mathbf{r}_0^i + \mathbf{I} \times \mathbf{r}_0^i\right)\right) \tag{6}$$

where $\mathbf{r}_0^i$ is the initial orientation for the ith grain. Thus the initial slip system α of grain i, represented in the sample coordinate system, can be determined by

$$\begin{aligned}\mathbf{m}_0^{i,\alpha} &= \mathbf{R}_0^i \mathbf{m}_{local}^\alpha \\ \mathbf{n}_0^{i,\alpha} &= \mathbf{R}_0^i \mathbf{n}_{local}^\alpha\end{aligned} \tag{7}$$

where $\alpha = 1, \ldots, 12$ for FCC materials and $\mathbf{m}_{local}^\alpha$ and $\mathbf{n}_{local}^\alpha$ are the slip direction and plane normal, respectively, in the local (crystal) coordinate system. $\mathbf{m}_0^{i,\alpha}$ and $\mathbf{n}_0^{i,\alpha}$ define the initial orientation of grain i and are needed for computing the resolved shear stresses and update the plastic deformation in the crystal plasticity simulation.

Although orientations are usually defined within the fundamental zone of Rodrigues space due to the crystal symmetry, the range of Rodrigues components are in essence from negative infinity to positive infinity. Thus, the vector $\boldsymbol{\tau}$ has no constraint. Our goal is to find a lower-dimensional space $\Gamma \subset \mathbb{R}^{d_2}$ as the surrogate space of $\mathscr{T}$.

For a microstructure that underwent through a sequence of deformation processes controlled by random variables $\boldsymbol{\omega} = \{\omega_1, \omega_2, \ldots\}$, its texture will also depends on $\boldsymbol{\omega}$. While the explicit relationship between $\boldsymbol{\tau}$ and $\boldsymbol{\omega}$ is not easy, neither necessary, to find, we adopt the Karhunen–Loève Expansion (KLE) to represent the random texture using a series of intermediate uncorrelated parameters $\boldsymbol{\eta}$, which are implicitly dependent on $\boldsymbol{\omega}$. Given a set of N texture samples, the unbiased estimate of the covariance matrix of these texture vectors is

$$\widetilde{\mathbf{C}} = \frac{1}{N-1}\sum_{i=1}^{N}(\boldsymbol{\tau}_i - \bar{\boldsymbol{\tau}})^T(\boldsymbol{\tau}_i - \bar{\boldsymbol{\tau}}), \bar{\boldsymbol{\tau}} = \frac{1}{N}\sum_{i=1}^{N}\boldsymbol{\tau}_i \tag{8}$$

$\boldsymbol{\tau}_i$ is the ith realization of $\boldsymbol{\tau} \in \mathscr{T}$ and N is the total number of known realizations, namely the sample number. The truncated Karhunen–Loève Expansion of the random vector $\boldsymbol{\tau}$ is then written as

$$\boldsymbol{\tau}(\mathbf{r},\boldsymbol{\omega}) = \bar{\boldsymbol{\tau}}(\mathbf{r},\boldsymbol{\omega}) + \sum_{i=1}^{d_2} \sqrt{\lambda_i}\boldsymbol{\phi}_i(\mathbf{r})\eta_i(\boldsymbol{\omega}) \tag{9}$$

where $\boldsymbol{\phi}_i$, λ_i are the ith eigenvector and eigenvalue of $\widetilde{\mathbf{C}}$, respectively; $\{\eta_i(\boldsymbol{\omega})\}$ is a set of uncorrelated random variables having the following two properties

$$\begin{aligned} &E(\eta_i(\boldsymbol{\omega})) = 0, \\ &E(\eta_i(\boldsymbol{\omega})\eta_j(\boldsymbol{\omega})) = \delta_{ij}, \quad i,j = 1,\ldots,d_2 \end{aligned} \tag{10}$$

and their realizations are obtained by

$$\eta_i^{(j)} = \frac{1}{\sqrt{\lambda_i}}\left\langle \boldsymbol{\tau}_j - \bar{\boldsymbol{\tau}}, \boldsymbol{\phi}_i \right\rangle_{l_2}, \quad j = 1,\ldots,N,\ i = 1,\ldots,d_2 \tag{11}$$

where $\langle\cdot,\cdot\rangle$ denotes the scalar product in $\mathbb{R}^N$. Since the covariance function is symmetric and positive definite, all the eigenvalues are positive real numbers and the eigenvectors are mutually orthogonal and they span the space in which $\boldsymbol{\tau}(\mathbf{r},\boldsymbol{\omega})$ belongs to. The summation in Eq. (9) is mean square convergent and usually truncated after few dominant terms, which preserve most information of the vector $\boldsymbol{\tau}$.

The truncated realizations of $\{\boldsymbol{\eta}^{(j)}\} \in \Gamma \subset \mathbb{R}^{d_2}$ are treated as reduced texture representations, which is analogous to the reduced grain size samples $\{\mathbf{y}_i\} \in \mathscr{A}$. The only constraint that we know about the random variables $\{\boldsymbol{\eta}^{(j)}\}$ is from Eq. (10). This distribution can be easily derived using Maximum Entropy Principle (MaxEnt) [9]. Only in a very few special cases, the uncorrelated Gaussian random variables are not independent [20] and our example is not in that category. Therefore, here we treat $\boldsymbol{\eta}$ as a set of independent random variables that are normally distributed around $\mathbf{0}$. A convenient method to transform $\boldsymbol{\eta}$ to random variables $\boldsymbol{\zeta}$ that are uniformly distributed within the hypercube $[0,1]^{d_2}$ is based on the Rosenblatt transformation [21]. The distribution of $\boldsymbol{\zeta}$ is in fact the cumulative distribution functions (CDF) of $\boldsymbol{\eta}$.

$$\begin{aligned} \zeta_1 &= \Phi_{\eta_1}(\eta_1) \\ \zeta_2 &= \Phi_{\eta_2|\eta_1}(\eta_2|\eta_1) = \Phi_{\eta_2}(\eta_2) \\ &\vdots \\ \zeta_{d_2} &= \Phi_{\eta_{d_2}|\eta_1\ldots\eta_{d_2}-1}(\eta_{d_2}|\eta_1\ldots\eta_{d_2}-1) = \Phi_{\eta_{d_2}}(\eta_{d_2}) \end{aligned} \tag{12}$$

where $\Phi(\cdot)$ is the standard normal CDF and in the current case is

$$\Phi_{\eta_i}(\eta_i) = \frac{1}{2}\left[1 + erf\left(\frac{\eta_i}{\sqrt{2}}\right)\right] \tag{13}$$

For a given point in the hypercube $\boldsymbol{\zeta} \in [0,1]^{d_2}$, its corresponding point $\boldsymbol{\eta}$ from the original distribution is naturally found to be

$$\eta_i = \Phi^{-1}(\zeta_i), \quad i = 1,\ldots,d_2 \tag{14}$$

which can immediately give us a texture vector using Eq. (9).

Based on the analysis above, each microstructure $\mathbf{h}$ (with both grain size and texture features) that belongs to the high-dimensional stochastic space $\mathscr{H} = \mathscr{M} \times \mathscr{T}$, can be presented by $\mathbf{l}(\mathbf{y},\boldsymbol{\eta})$ in the low-dimensional surrogate space $\mathscr{L} = (\mathscr{A} \times \Gamma) \subset \mathbb{R}^d$ $(d = d_1 + d_2)$.

A mapping from $\mathscr{L}$ to $\mathscr{H}$ can be constructed for sampling allowable microstructure features. Define the stochastic model for the feature variation as $\mathscr{F}^{-1}(\xi) : \mathscr{L} \to \mathscr{H}$, where $\boldsymbol{\xi} = \{\xi_1,\ldots,\xi_d\}$ is a random vector chosen from $\mathscr{L}$. This low-dimensional stochastic model $\mathscr{F}^{-1}$ for the microstructure is the input to the SPDEs defining the crystal plasticity problem. For the grain size feature, this mapping is described in Section 3.2; for texture, the mapping is directly performed by Eq. (9), where $\mathscr{F}^{-1}(\boldsymbol{\eta}) : \boldsymbol{\eta} \to \boldsymbol{\tau}$.

Mapping the low-dimensional space to a hypercube having the same dimensionality [6], the uncertainty of the mechanical property of the microstructure can be efficiently investigated using the Adaptive Sparse Grid Collocation (ASGC) method. It is a stochastic collocation procedure that solves stochastic partial differential equations (SPDEs) by computing the solution at various sample points, $\boldsymbol{\xi}$, from this space, $\mathscr{L}$. Each of the sample points corresponds to a microstructure that can be interrogated to evaluate its mechanical response. The sparse grid collocation approach will then create an interpolant of the mechanical response in the d-dimensional stochastic space of the random microstructures.

5. Sparse grid collocation

In the previous sections, the grain size and texture of a polycrystalline microstructure have been reduced to a set of lower-dimensional representations as the input to stochastic simulation. A highly efficient, stochastic collocation based solution strategy is used to solve for the evolution of mechanical response. This section briefly reviews the adaptive sparse grid collocation method for solving SPDEs. For details, the interested reader is referred to [10].

The basic idea of sparse grid collocation is to approximate the multi-dimensional stochastic space $\mathscr{L}$ using interpolating functions on a set of collocation points $\{\boldsymbol{\xi}_i\}_{i=1}^{M} \in \mathscr{L}$. The collocation method collapses the multi-dimensional problem (based on the Smolyak algorithm) to solving M (M is the number of collocation points) deterministic problems. One computes the deterministic solution at various points in the stochastic space and then builds an interpolated function that best approximates the required solution. Notice, during the process, the mapping $\mathscr{F}^{-1}$ from low-dimensional surrogate $\mathscr{L}$ to high-dimensional microstructural space $\mathscr{H}$ needs to be implemented, so that the deterministic solver can work.

In the context of incorporating adaptivity, Newton-Cotes grid is utilized with equidistant support nodes. Hierarchical basis is used in constructing the interpolant. The interested function $u(t,\boldsymbol{\xi})$ can be approximated by

$$\hat{u}_{d,q}(t,\boldsymbol{\xi}) = \sum_{\|\mathbf{i}\| \leqslant d+q} \sum_{\mathbf{j} \in B_i} \omega_{\mathbf{j}}^{\mathbf{i}}(t) \cdot a_{\mathbf{j}}^{\mathbf{i}}(\boldsymbol{\xi}) \tag{15}$$

The mean of the random solution is evaluated as:

$$E(\hat{u}_{d,q}(t)) = \sum_{\|\mathbf{i}\| \leqslant d+q} \sum_{\mathbf{j} \in B_i} \omega_{\mathbf{j}}^{\mathbf{i}}(t) \cdot \int_{\mathscr{L}} a_{\mathbf{j}}^{\mathbf{i}}(\boldsymbol{\xi}) d\boldsymbol{\xi} \tag{16}$$

where q is the depth (level) of sparse grid interpolation and d is the dimensionality of stochastic space. B_i is a multi-index set. $\omega_{\mathbf{j}}^{\mathbf{i}}$ is the hierarchical surplus, which is the difference between the function value $u(t,\boldsymbol{\xi})$ at the current point $\boldsymbol{\xi}$ and interpolation value $\hat{u}_{d,q-1}(t,\boldsymbol{\xi})$ from the coarser grid in the previous level. $a_{\mathbf{j}}^{\mathbf{i}}$ is the d-dimensional multilinear basis functions defined by tensor product. For the estimation of higher-order moments (kth-order) of the function of interest, we only need to change u to u^k. The function of interest u and its interpolation $\hat{u}$ in the current work are the volume average equivalent stress of a polycrystalline microstructure at an equivalent strain of 0.2.

With increasing level of interpolation, new support nodes are added to the hypercube if the error indicator

$$\gamma_{\mathbf{j}}^{\mathbf{i}} = \frac{\|\omega_{\mathbf{j}}^{\mathbf{i}} \cdot \int_{\mathscr{L}} a_{\mathbf{j}}^{\mathbf{i}}(\boldsymbol{\xi}) d\boldsymbol{\xi}\|_{L_2}}{\|E_{\|\mathbf{i}\|-d-1}\|_{L_2}} \tag{17}$$

is larger than a threshold ϵ. The error indicator $\gamma_{\mathbf{j}}^{\mathbf{i}}$ measures the contribution of each term in Eq. (16) to the integration value (mean of the interpolated function) relative to the overall integration value computed from the previous interpolation level. The convergence properties (e.g. error versus threshold ϵ and error versus number of collocation points for a given ϵ) are discussed in [10].

After the ASGC has been performed, the solutions of the SPDEs, namely the mechanical response of the random microstructures

has been computed as an interpolant in the stochastic support space that defines the microstructure variability. Using this high-dimensional interpolant of the mechanical response, one can compute statistical quantities of interest such as realizations, moments and the probability density function (PDF) using kernel density estimation [11].

6. Deterministic solver

We are interested to compute the variability of the macroscopic mechanical response of polycrystalline microstructures subjected to homogenized compression in the presence of uncertainty in grain size and texture. The deterministic solver is based on a rate-independent crystal plasticity constitutive model developed in [19]. A multiplicative decomposition of the deformation gradient into an elastic and plastic part, $\mathbf{F} = \mathbf{F}^e\mathbf{F}^p$, is used. By comparing the resolved shear stress with the slip resistance on specific slip system, active slip systems can be determined, which control the hardening of the crystals. The grain size effect is incorporated by explicitly introducing a grain size parameter into the Taylor hardening law [22]:

$$\hat{\tau} - \hat{\tau}_0 = \alpha\mu b\sqrt{\rho} \tag{18}$$

where

$$\dot{\rho} = \sum_{\kappa}\left\{\frac{1}{L_g b} + k_1\sqrt{\rho} - k_2\rho\right\}|\dot{\gamma}^{\kappa}| \tag{19}$$

The first term in Eq. (19) represents a geometric storage due to lattice incompatibility, describing the grain boundary hardening. L_g is the grain size parameter, which is effectively the equivalent diameter of the grain [23]. $\hat{\tau}$ is the single crystal flow strength, $\hat{\tau}_0$ is the initial yield strength, α is a constant usually chosen to be 1/3, b is the Burgers vector, μ is the shear modulus, ρ is the density of dislocations, and $\dot{\gamma}^{\kappa}$ is the strain rate of slip system κ. k_1 and k_2 are constants that can be determined from observations. The second term in Eq. (19) describes storage through a statistical measure of forest dislocation, describing the dislocation interaction hardening inside grains. The last term in Eq. (19) represents a dynamic recovery rate that renders dislocation segments inactive as they rearrange themselves [22].

The elastic and plastic deformation gradients can also be updated after calculating the incremental shear strain, which is determined by setting the resolved shear strain equal to the slip resistance. The Cauchy stress for each grain is calculated by

$$\mathbf{T} = \mathscr{C}^e\mathbf{E}^e \tag{20}$$

where $\mathbf{E}^e = \frac{1}{2}(\mathbf{F}^{eT}\mathbf{F}^e - \mathbf{I})$ is the strain tensor and $\mathscr{C}^e$ is the fourth-order elasticity tensor expressed in the microstructure coordinate system.

The deformation of the microstructure follows the Taylor hypothesis, in which all grains are assumed to be subject to the same deformation gradient. Under Taylor hypothesis, a realization of the microstructure is not necessary and the interactions between grains are neglected. This is a commonly used method for computing the homogenized macroscopic properties of materials in a stochastic simulation due to its high computational efficiency. Macroscopic properties, such as stress and strain, are computed as the volume average of the microscopic values for different grains. For example, the macroscopic Cauchy stress $\overline{\mathbf{T}}$ and average plastic rate of deformation $\overline{\mathbf{D}}$ are calculated in the following form:

$$\overline{\mathbf{T}} = \langle\mathbf{T}\rangle = \frac{1}{V(\mathscr{B})}\int_{V(\mathscr{B})}\mathbf{T}\,dV \tag{21}$$

$$\overline{\mathbf{D}} = \langle\mathbf{D}^p\rangle = \frac{1}{V(\mathscr{B})}\int_{V(\mathscr{B})}\mathbf{D}^p\,dV \tag{22}$$

Accordingly, the macroscopic Von-Mises equivalent stress and equivalent strain are calculated in the form of

$$\bar{\sigma}_{eff} = \sqrt{\frac{3}{2}\overline{\mathbf{T}}'\cdot\overline{\mathbf{T}}'} \tag{23}$$

where $\overline{\mathbf{T}}'$ is the deviatoric part of $\overline{\mathbf{T}}$, and

$$\bar{\varepsilon}_{eff} = \int_0^t\sqrt{\frac{2}{3}\overline{\mathbf{D}}\cdot\overline{\mathbf{D}}}\,dt \tag{24}$$

Utilizing this deterministic solver, several cases were considered and compared with available experimental data. The microstructure of interest consists of 64 grains each of which is assigned a random orientation. Nickel is selected as the material with parameters in Eqs. (18) and (19) being $\tau_0 = 20$ MPa, $b = 2.49\times10^{-7}$ mm, $k_1 = 1.15\times10^5$ mm^{-1}, $k_2 = 3.14$, and the three independent elastic constants are $C_{11} = 247$ GPa, $C_{12} = 147$ GPa, $C_{44} = 125$ GPa [22,24]. By varying the domain size of the microstructure, the effective stress of different mean grain size microstructures subjected to compression are computed and plotted at a series of strains (from 5% to 20%). Comparing with the experimental data [22,25], we found our results to be consistent with experiments (Fig. 6). Although the restricted assumption in the Taylor model raises the material strength to some extent, the superior computation efficiency makes this method highly preferable in stochastic simulations. The variability of the macroscopic equivalent stress at specific strain under the same deformation history is of interest in this paper.

We assume here that the grain size distribution is independent of texture. Therefore, the correlation of grain size and orientation is not considered during sampling. We simply first sample the grain sizes according to the given statistical constraints, such as mean size and higher moments, and then sample the grain orientations in the Rodrigues space. A microstructure is constructed by combining these two feature realizations. However, the effects of grain size and texture on mechanical properties of a microstructure are coupled. The reason is that a macroscopic property is calculated as the volume average of microscopic properties,

$$\langle\Gamma\rangle = \frac{1}{V}\sum_i^n\Gamma_i V(\mathbf{r}_i) \tag{25}$$

in which $\Gamma_i = \Gamma(\mathbf{r}_i)$ is the property of grain i having orientation $\mathbf{r}_i$ and $V(\mathbf{r}_i)$ is its volume. n is the number of total grains, V is the volume of the microstructure. Therefore, if a microstructure contains

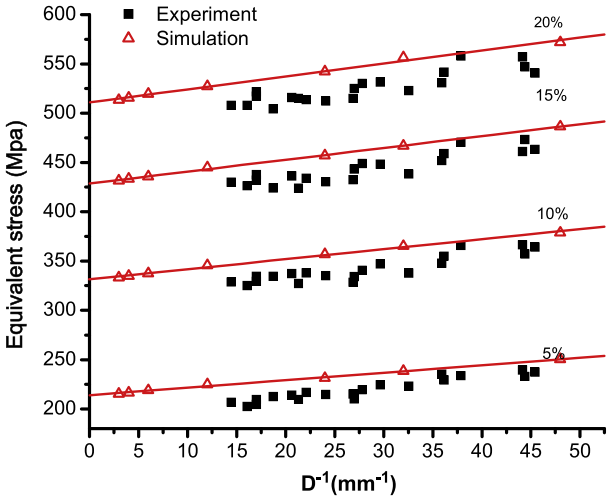

Fig. 6. A comparison of the simulated and experimental results.

grains of different sizes corresponding to the same orientation, the average property varies. For example, consider two microstructures having the same texture vector Eq. (5). If the two microstructures have different grain size distribution, the volume of grains associated with the same orientation will be different. As a result, the overall mechanical properties of these two microstructures will be different. This coupled effect is taken automatically into consideration in the present analysis.

7. Numerical examples

In this section, several examples are presented to study the statistics of mechanical response of polycrystalline microstructures based on the model reduction techniques and sparse grid collocation method introduced above. The deterministic solver adopts the polycrystal plasticity constitutive model introduced earlier. The macroscopic equivalent stress is averaged over the microstructure domain following the Taylor hypothesis. In the following numerical examples, the mechanical response of FCC nickel microstructures subjected to homogeneous compression is examined given various grain size and texture information.

The methodologies that are used in solving this stochastic problem are introduced in the previous sections. Here, we summarize the main procedure of addressing the examples of interest.

(1) Generate a number of grain size samples $\{\mathbf{x}_i\} \in \mathscr{M}$, $i = 1, \ldots, N$ according to certain information (prescribed mean size, second- and third-order moments, etc.). The given input microstructures satisfy the same constraints.
(2) Utilize NLDR to reduce the dimensionality of the grain size samples. Their low-dimensional representations are $\{\mathbf{y}_i\} \in \mathscr{A}$, $i = 1, \ldots, N$. The optimal dimensionality of the lower space $\mathscr{A}$ is linked to the rate of convergence of the length functional of the minimal spanning tree of the geodesic distance matrix of the unordered data points in the high-dimensional space [6]. A convex hull is constructed as the envelope of the reduced points.
(3) Assign a given texture to the given set of microstructures. Put them through a sequence of deformation processes that are controlled by several random processing variables $\boldsymbol{\omega}$. The resultant textures are utilized to construct initial random texture space $\mathscr{T}$ for the stochastic polycrystal plasticity problem.
(4) Perform KLE on texture samples, $\{\boldsymbol{\tau}_i(\boldsymbol{\omega})\}$, $i = 1, \ldots, N$. The low-dimensional representations $\{\boldsymbol{\eta}^{(i)}\} \in \Gamma$ can be obtained by truncating the eigen-spectrum to a desired level.
(5) Combine the reduced grain size and texture to form the low-dimensional surrogate of feature space of microstructures, which is the stochastic input to the sparse grid collocation SPDE solver.
(6) Use the ASGC method to construct the stochastic solution. This method solves the deterministic problem at various collocation points ξ on the stochastic space and constructs an interpolation based approximation to the stochastic solution. For a given set of stochastic collocation points, the corresponding microstructures of these points can be reconstructed (by the mapping $\mathscr{F}^{-1} : \mathscr{L} \to \mathscr{H}$) and used as inputs in the solution of the corresponding crystal plasticity boundary value problem (compression test). For each of these deterministic problems, the elasto-plastic mechanical response is computed by the Taylor homogenization. The ASGC method constructs the stochastic interpolant of the mechanical response using the deterministic responses for the appropriately selected sparse grid collocation points.
(7) After the corresponding stochastic plasticity problem has been solved, the final equivalent stress for any other microstructure realization in the stochastic support space can be calculated using the hierarchical interpolating functions. The probability distribution of the final equivalent stress at strain 0.2 is constructed using kernel smoothing density estimation on the histogram of realizations.

7.1. Example 1

In the first example, 1000 microstructure samples are first generated. Each sample contains 54 grains whose volume is uniformly distributed in the interval between 0.0037 mm^3 and 0.0333 mm^3. The mean grain volume of each microstructure is controlled to be 0.0185 mm^3, while higher-order moments are free to vary. These samples are used as the input database of grain size feature. By applying the NLDR method (Section 2), we first construct the geodesic distance matrix between points and then map them to a low-dimensional space through Multi-Dimensional Scaling (MDS) and Isomap. The number of nearest neighbors is set to be 10. The intrinsic dimensionality d_1 of the low-dimensional space is estimated by linking to the convergence of the length functional of the minimal spanning tree (MST) of the neighborhood graph defined by geodesic distance matrix [6]. To be specific, for various sizes of samples (varying from 20 to 1000), points were randomly picked from the set of samples. The minimal spanning tree of these sample sets was computed. The length functional of the MST was computed for each of these sample sets. The optimal dimensionality of the low-dimensional set is related to the slope of the line representing the relationship between the length functional and the sample number (in logarithm form). The slope is computed using a least squares fit and found to be $a = 0.6973$. The reduced dimensionality is estimated using $d_1 = 1/(1-a)$ (Section 2), which is rounded to $d_1 = 3$ (Fig. 7). In this way, the original 54 dimensional grain size representation is reduced to 3.

The prescribed texture samples are obtained through a series of random processing on an initially arbitrarily generated sample. To be specific, an arbitrary texture consisted of 54 random orientations was first generated and assigned to 1000 microstructure samples. Then, these microstructures were input into a sequence of deformation modes controlled by two independent random variables ω_1 and ω_2.

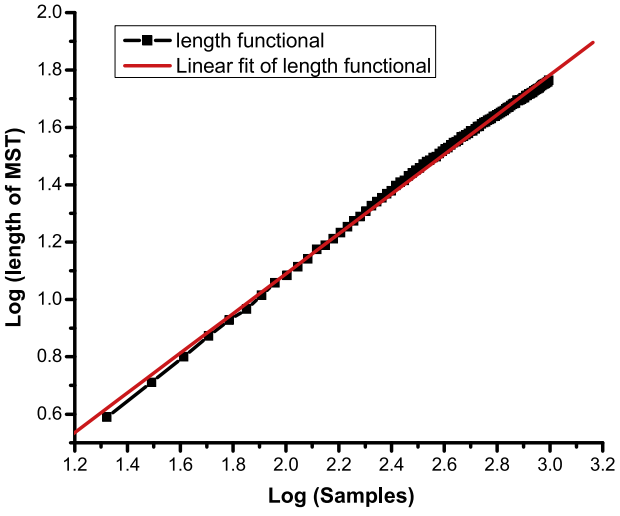

Fig. 7. Plot of the length functional of the MST with respect to various sample sizes.

$$\mathbf{L} = \omega_1 \begin{bmatrix} 0 & 0 & 0 \\ 0 & 1 & 0 \\ 0 & 0 & -1 \end{bmatrix} + \omega_2 \begin{bmatrix} 0 & -1 & 0 \\ 1 & 0 & 0 \\ 0 & 0 & 0 \end{bmatrix} \tag{26}$$

where random variables ω_1 and ω_2 determine the deformation rate $\mathbf{L}$ of different modes and vary from $-0.002\ s^{-1}$ to $0.002\ s^{-1}$. At each time step, the deformation of the microstructure is controlled by the combination of these two modes, but for different samples, the combination is different in terms of the deformation rates ω_1 and ω_2. At the end of 500 s, the 1000 resultant textures were collected as the input texture database to the stochastic problem. With these texture samples, the unbiased estimate of the covariance matrix $\widetilde{\mathbf{C}}$ is constructed. We then apply KLE (Section 4) on the covariance matrix and set the energy cutoff to be 90% – truncate the eigenvalue and eigenvector number d_2 when the energy captured by the first d_2 eigenvalues is larger than 90%. Fig. 8 shows that the first two eigenvalues of the covariance matrix captured 93.1% of the total energy (summation of all eigenvalues). Therefore, the dimensionality of the reduced initial texture is chosen to be 2.

A three-dimensional convex hull corresponding to low-dimensional grain size representation is constructed with 88 faces and mapped to unit hypercube $[0,1]^3$ [6], and the low-dimensional texture representation is also mapped to a two-dimensional hypercube $[0,1]^2$. Assuming grain size and texture features are independent, the complete low-dimensional surrogate of microstructure is five-dimensional. Therefore, a five-dimensional hypercube can be constructed whose first three dimensions correspond to grain size and the last two dimensions correspond to texture. The adaptive sparse grid collocation (ASGC) method is used with a sparse grid defined on this hypercube $[0,1]^5$ to investigate the mechanical response uncertainty due to the variation of grain size and texture. The cutoff of error indicator Eq. (17) controlling the interpolation error is set to be 0.001. Each realization within the hypercube can be transformed to the low-dimensional space and therefore mapped to a microstructure feature set (Sections 3.2 and 4). The mechanical response of the new microstructure was then computed using the Taylor model deterministic solver (Section 6). In this example, homogeneous compression is applied to the microstructure. The velocity gradient is

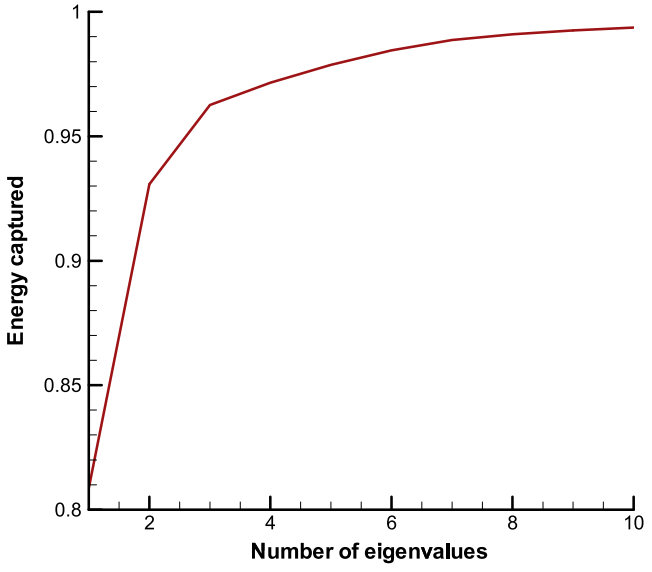

Fig. 8. The 'energy' captured by the most significant eigenvalues.

$$\mathbf{L} = 0.002\ s^{-1} \begin{bmatrix} 0.5 & 0 & 0 \\ 0 & 0.5 & 0 \\ 0 & 0 & -1 \end{bmatrix} \tag{27}$$

The final equivalent strain is $\varepsilon = 0.2$. The homogenized macroscopic equivalent stresses corresponding to this strain is the primary variable that is interpolated in the stochastic space using a level 8 of interpolation. Thousand one hundred and ninty-two collocation points are adaptively generated. The mean final equivalent stress is found to be 539.159 MPa and the standard deviation is 10.471 MPa. As mentioned, the ASGC method decomposes the multi-dimensional stochastic problem into solving a number of deterministic problems. Thus, the deterministic solver is called at each collocation point. The deterministic solver (here, the Taylor model crystal plasticity solver) estimates the relation between the equivalent stress and equivalent strain and records the history of deformation process in a stress–strain curve. The variation in the stress–strain response is shown in Fig. 9a, where the bars represent the standard deviation of the equivalent stress for the corresponding equivalent strain. Constructing the interpolant of the final equivalent stress (at strain equal to 0.2), we can obtain the distribution of the final stress by sampling uniformly from the hypercube. According to Eq. (15), given a point located in the hypercube, we can find a stress corresponding to it. Generate sufficient samples (in this case, 10,000 points are generated from the interpolant), a histogram of the final stress is obtained. Utilizing kernel smoothing density estimation [11], the PDF of the final equivalent stress is plotted in Fig. 9b.

7.2. Example 2

In the second example, the initial texture samples are generated through a three-random variable process, in which a homogeneous compression component is added to the previous two modes (Eq. (28)). After KLE, the lower-dimensional representation is cut off at $d_2 = 4$, where 91.8% energy is captured. The grain size samples are the same with Example 1, so that the final low-dimensional space is 7. We aim at investigating the initial texture uncertainty dependence of the mechanical response.

$$\mathbf{L} = \omega_1 \begin{bmatrix} 0.5 & 0 & 0 \\ 0 & 0.5 & 0 \\ 0 & 0 & -1 \end{bmatrix} + \omega_2 \begin{bmatrix} 0 & 0 & 0 \\ 0 & 1 & 0 \\ 0 & 0 & -1 \end{bmatrix} + \omega_3 \begin{bmatrix} 0 & -1 & 0 \\ 1 & 0 & 0 \\ 0 & 0 & 0 \end{bmatrix} \tag{28}$$

Following the similar procedure as in Section 7.1, 7146 nodes are adaptively generated for a level 8 sparse grid collocation. The mean stress was computed to be 540.148 MPa and the standard deviation 13.304 MPa. It comes to our notice that although the mean stress is almost the same as in the previous example, the standard deviation is increased, which means the variance of the equivalent stress is enlarged. The stress–strain curve variation and final stress distribution are collected and constructed in Fig. 10. From this figure, a wider distribution of the mechanical response is observed, which implies that the randomness of the mechanical response increased because of the additional randomness in texture.

7.3. Example 3

The first two examples demonstrated the mechanical response variability due to texture uncertainty. This example considers the grain size effect on mechanical properties. The mean grain volume is preserved at 0.0185 mm^3, whereas the second-order moment is set to be $3.704 \times 10^{-4}\ mm^6$. Compared with Example 1, where the second-order moment is various and mostly around $4.10 \times$

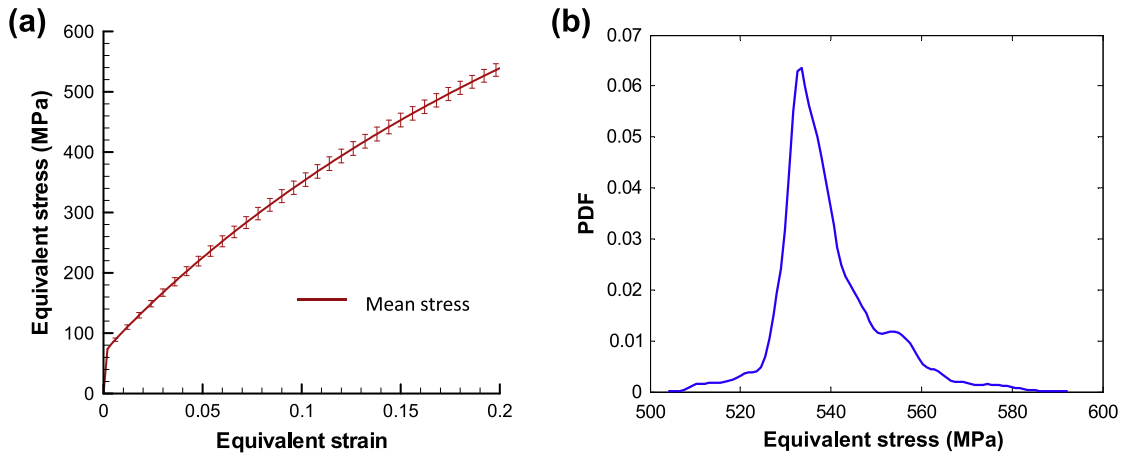

Fig. 9. (a) Variation in stress–strain response due to uncertainty in grain size and initial texture. The random texture was generated from the deformation process defined in Eq. (27). The bars represent the standard deviation of the effective stress for the corresponding effective strain. (b) PDF of the final equivalent stress of the microstructures having the same mean size.

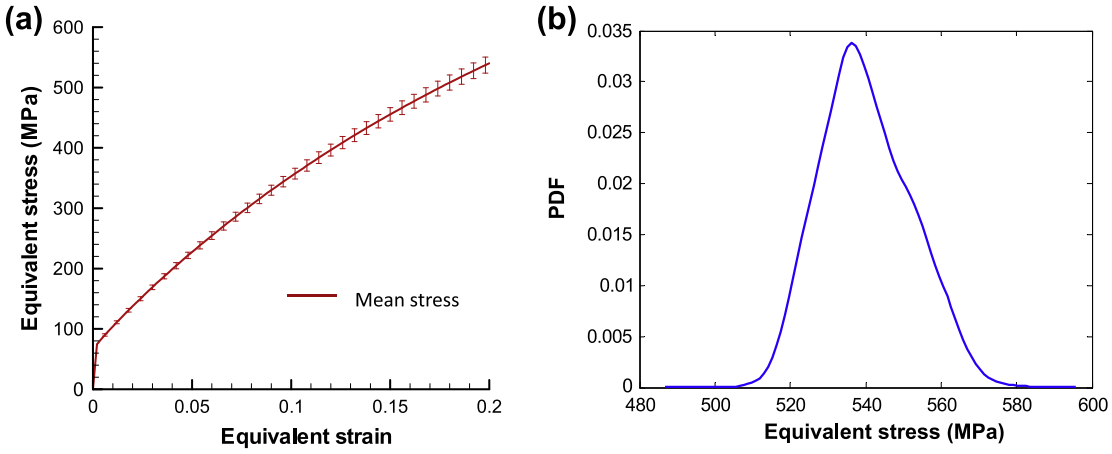

Fig. 10. (a) Variation in stress–strain response due to the effect of uncertainty in grain size and initial texture. The random texture was generated from the deformation process defined in Eq. (28). The bars represent the standard deviation of effective stress for the corresponding effective strain. (b) PDF of the final equivalent stress of the microstructures having the same mean size.

$10^{-4}\,\mathrm{mm}^6$, the microstructures in this example have a narrow grain size distribution. Performing NLDR, the best fit dimensionality d_1 of the low-dimensional space is still 3.

We select the initial texture the same as in the first example that was generated from Eq. (26). Similar estimation process is conducted and the mechanical response is analyzed up to level 8 with 936 adaptively generated collocation points. The mean final equivalent stress and standard deviation are 537.918 MPa and 8.957 MPa, respectively. In the stress–strain response variation (Fig. 11a) and final stress distribution (Fig. 11b), a sharper distribution is observed. The final stresses corresponding to narrow grain size distribution are more concentrated around the mean value.

7.4. Example 4

In this section, we constrain the grain size distribution of microstructure samples through three moments. Keeping the first two moments identical with those in Example 3, the third-order moment constraint is added with the value $8.637 \times 10^{-6}\,\mathrm{mm}^9$. This value is larger than the average third-order moment ($7.86 \times 10^{-6}\,\mathrm{mm}^9$) when only the first two moments are constrained. This variance results that most grain sizes in a microstructure are close but smaller than the mean size, while a few grain sizes are much larger than the others. If the third-order moment is set to a higher value, the variation of the grain size will be quite small or even cannot be captured among the microstructure samples. The resulting microstructures tend to have the same grain size distribution. A comparison of sorted grain size vectors among three microstructure samples whose grain size distributions are constrained by different number of moments are demonstrated in Fig. 12. We can observe that the microstructure constrained by only the mean size tends to have almost evenly distributed grain sizes. Grain sizes of the one constrained by two moments are more concentrated around the mean size. In the case that three moments are constrained, most grain sizes are a little smaller than the mean size, while a couple of grains have unusual large values.

As more constraints are applied to the grain size distribution, the underlying correlation is increased. Performing NLDR on this set of sorted grain size vectors, we obtain the optimal dimensionality of the grain size feature to be 2. Combining the reduced grain size vectors with texture (the same as Example 1), the low-dimensional space has only four dimensions. The governing stochastic equations for compression are solved through ASGC up to level 8 with 798 collocation points. The mean final equivalent stress is found to be 539.543 MPa and the standard deviation is 8.974 MPa. The stress–strain curve variance and final stress

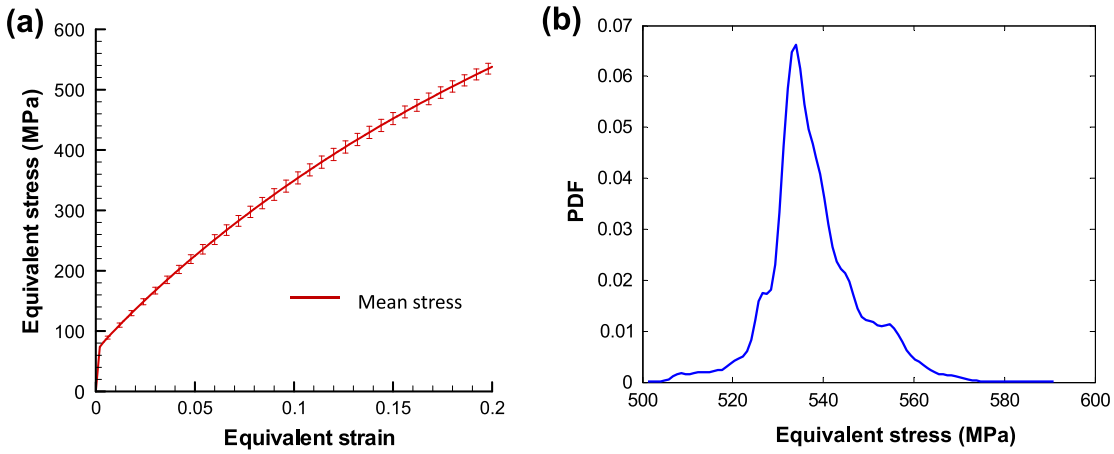

Fig. 11. (a) Variation in stress–strain response due to the effect of uncertainty in grain size and initial texture. The input microstructures have fixed mean grain size and second-order grain size moment, whereas their texture is defined from the process in Eq. (26). The bars represent the standard deviation of effective stress for the corresponding effective strain. (b) PDF of the final equivalent stress of the microstructures.

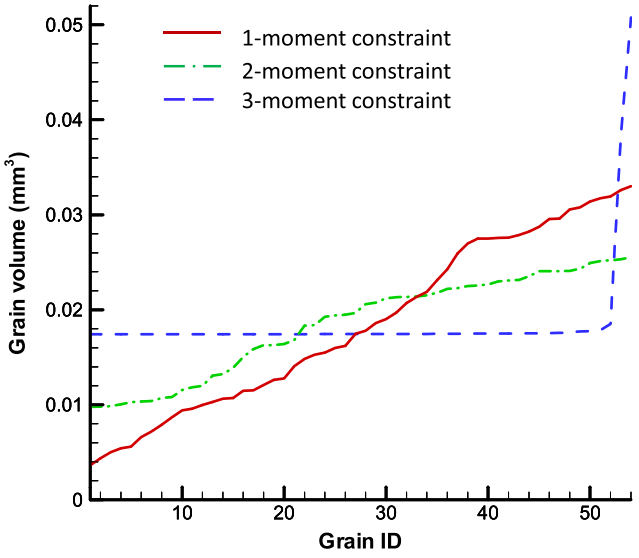

Fig. 12. Three microstructure samples whose grain size distributions are constrained by different number of moments. The first case is constrained by mean volume 0.0185 mm^3; the second is constrained by the same mean volume and the second-order moment 3.704×10^{-4} mm^6; the last case is constrained by a third-order moment 8.637×10^{-6} mm^9 in addition to the first two moments.

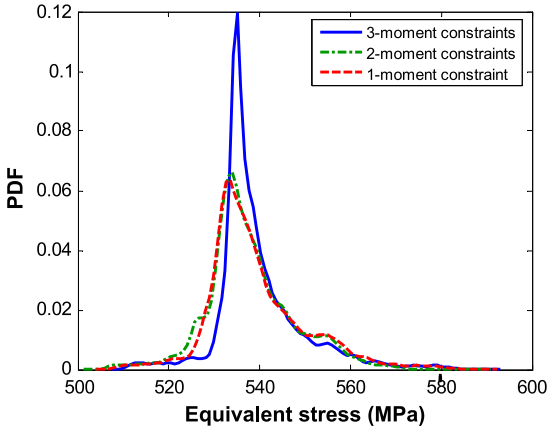

Fig. 14. Final stress distribution of microstructures whose grain size distributions are constrained by different number of moments: mean grain volume 0.0185 mm^3 (dashed); mean grain volume 0.0185 mm^3 and second-order moment 3.704×10^{-4} mm^6 (dash-dot); mean grain volume 0.0185 mm^3, second-order moment 3.704×10^{-4} mm^6, and third-order moment 8.637×10^{-6} mm^9 (solid).

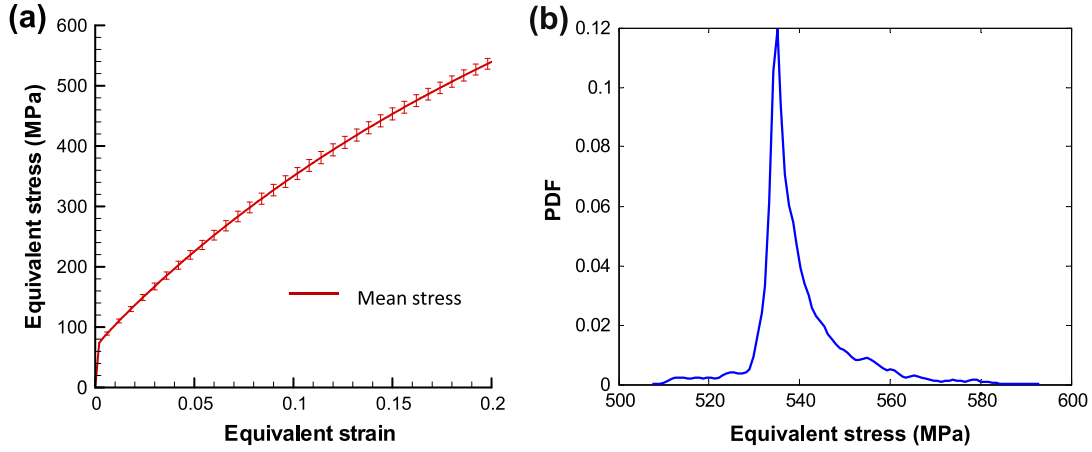

Fig. 13. Case of microstructures having the same mean size, second-order and third-order moments. Variation in stress–strain response due to the effect of uncertainty in grain size and initial texture. The bars represent the standard deviation of effective stress for the corresponding effective strain. (b) PDF of the final equivalent stress.

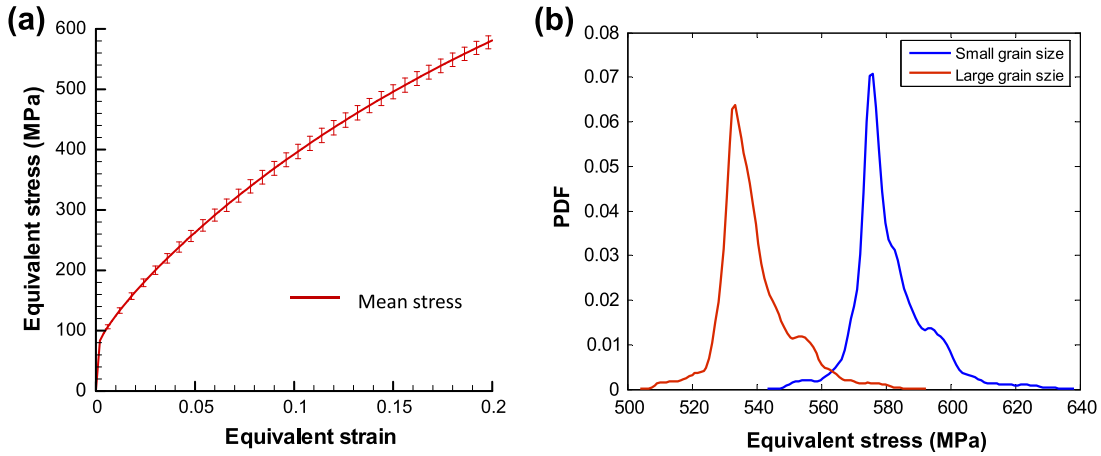

Fig. 15. (a) Variation in stress–strain response due to the effect of uncertainty in grain size and initial texture. The mean grain size is 1.85×10^{-5} mm^3. The bars represent the standard deviation of the effective stress for the corresponding effective strain. (b) Final stress distribution of microstructures having different mean grain size.

distribution are plotted in Fig. 13. Although the variance is almost the same as in Example 3, the distribution of the final stress is more concentrated. A comparison between the final stress distribution of these three cases are shown in Fig. 14.

7.5. Example 5

In the last example, the volume of the microstructure is reduced to 0.001 mm^3 (compared to previously 1 mm^3 domain). In this way, the mean effective diameter of grains is decreased to 1/10 of the first example. The volume of individual grains now distributed within 3.7×10^{-6} mm^3 to 3.33×10^{-5} mm^3 interval. Only the mean grain size is constrained. This example meant to study the microstructure mean grain size effect on the mechanical response distribution. The smaller the grain size, the higher the equivalent stress should be induced at the same strain.

Fig. 15a shows the stress–strain curve variation. The mean value of the final stress is 580.996 MPa (raised by about 40 MPa) and the standard deviation is 10.634 MPa (close to the standard deviation 10.471 MPa in Example 1). Fig. 15b compares the final stress distributions of different mean grain size. Both cases have similar shape while the one with smaller grain size has higher mean value.

8. Conclusions

In this paper, the effect of multiple sources of uncertainty on macroscopic mechanical response is studied. A microstructure was considered as a combination of random fields consisted of grain size and texture. Given a set of microstructure samples as the realization of this random field, dimensionality reduction techniques were applied to find their underlining correlations. A nonlinear model reduction based on Isomap was performed on grain size variables and Karhunen–Loève Expansion was adopted to reduce the texture dimensionality. The dimensionality of the random field was successfully reduced from 216 to less than 7. Adaptive sparse grid collocation was then introduced to sample new microstructures from the low-dimensional space. The elasto-plastic mechanical response of the microstructures satisfying given information was computed and its distribution is constructed. The effect of texture and grain size randomness is studied. It shows that the model reduction techniques greatly simplified the representation of random microstructure features, while the significant characters can be preserved. The propagation of uncertainty in microstructure evolution enables one to provide the prediction on macroscopic mechanical response. The distribution of final stress and stress–strain curve provide important guidance in material design and process, when certain grain size and texture information is known.

The sparse grid approach constructed an interpolant of the mechanical response in the stochastic space of grain size distribution and texture. This interpolant allows the user to compute with controllable interpolation error the response of any other microstructure in the class of the given microstructures. This cannot be possible with alternative approaches as for example when using the Maximum Entropy (MaxEnt) approach with the given data. In addition, modeling the texture uncertainty using MaxEnt is computationally an intractable task.

In this work, the mechanical response was analyzed using the Taylor hypothesis which provides fast but less accurate results. In the Taylor model, the deformation of the microstructure is constrained to be identical in all grains and this leads to an over-estimation on the mechanical response. A finite element based approach assuming homogeneous deformation on the boundary is a more interesting approach to consider in the future as it captures higher-order texture effects (location and arrangement of grains).

Acknowledgements

We acknowledge support from the Computational Mathematics program of AFOSR (Grant F49620-00-1-0373), the Materials Design and Surface Engineering program of the NSF (award CMMI-0757824), the Mechanical Behavior of Materials program Army Research Office (proposal to Cornell University No. W911NF0710519) and an OSD/AFOSR MURI09 award to Cornell University on uncertainty quantification. This research was supported in part by the National Science Foundation through TeraGrid resources provided by NCSA under Grant number TG-DMS090007.

References

[1] V. Sundararaghavan, N. Zabaras, International Journal of Plasticity 22 (2006) 1799.
[2] V. Sundararaghavan, N. Zabaras, Statistical Analysis and Data Mining 1 (5) (2009) 306–321.
[3] S. Sankaran, N. Zabaras, Acta Materialia 55 (7) (2007) 2279.
[4] N. Zabaras, S. Sankaran, An information-theoretic approach to stochastic materials modeling, IEEE Computing in Science and Engineering (CiSE) (2007) 50 (special issue of 'Stochastic Modeling of Complex Systems', D.M. Tartakovsky, D. Xiu (eds.)).
[5] B. Ganapathysubramanian, N. Zabaras, Journal of Computational Physics 226 (2007) 326.

[6] B. Ganapathysubramanian, N. Zabaras, Journal of Computational Physics 227 (2008) 6612.
[7] S. Acharjee, N. Zabaras, Acta Materialia 51 (2003) 5627–5646.
[8] S. Ganapathysubramanian, N. Zabaras, Computer Methods in Applied Mechanics and Engineering 193 (2004) 5017–5034.
[9] B. Kouchmeshky, N. Zabaras, Computational Materials Science 47 (2009) 342–352.
[10] X. Ma, N. Zabaras, Journal of Computational Physics 228 (2009) 3084.
[11] A.W. Bowman, A. Azzalini, Applied Smoothing Techniques for Data Analysis, Oxford University Press, 1997.
[12] J.T. Kent, J.M. Bibby, K.V. Mardia, Multivariate Analysis (Probability and Mathematical Statistics), Elsevier, 2006.
[13] S.T. Roweis, L.K. Saul, Science 290 (2000) 2323.
[14] V. deSilva, J.B. Tenenbaum, Advances in Neural Information Processing Systems 15 (2003) 721.
[15] J. Tenenbaum, V. DeSilva, J. Langford, Science (2000).
[16] A Global Geometric Framework for Nonlinear Dimensionality Reduction, freely downloadable software available at <http://isomap.stanford.edu/>.
[17] C.E. Krill III, L.-Q. Chen, Acta Materialia 50 (2002) 3057.
[18] A. Kumar, P.R. Dawson, Acta Materialia 48 (2000) 2719–2736.
[19] L. Anand, M. Kothari, Journal of Mechanics and Physics of Solids 4 (1996) 525–558.
[20] E.L. Melnick, A. Tenenbein, The American Statistician 36 (4) (1982) 372–373.
[21] M. Rosenblatt, The Annals of Mathematical Statistics 23 (1952) 470–472.
[22] A.J. Beaudoin, A. Acharya, S.R. Chen, D.A. Korzekwa, M.G. Stout, Acta Metallurgica 48 (2000) 34093423.
[23] U.F. Kocks, H. Mecking, Progress in Materials Science (2003) 171–273.
[24] W. Li, N. Zabaras, Computational Materials Science 44 (2009) 1163–1177.
[25] T. Narutani, J. Takamura, Acta Metallurgica et Materialia 39 (1991) 2037–2049.